

Numerical study of TRISO particles with random size and location distribution in cuboid and cylindrical matrix: A validation for two-regime heat conduction model



Chunxi Wu ^b, Guitao Yang ^b, Wei Zhang ^b, Xianglong Guo ^b, Maolong Liu ^{a,*}

^a Institute of Modern Physics, Fudan University, Shanghai 200433, PR China

^b School of Nuclear Science and Engineering, Shanghai Jiao Tong University, Shanghai 200240, PR China

ARTICLE INFO

Keywords:

TRISO fuel particles
Numerical simulation
Random distribution
Heat conduction model

ABSTRACT

During reactor operation, the precise size values or specific size distribution of tri-structural isotropic (TRISO) fuel particles randomly dispersed within the fully ceramic microencapsulated (FCM) fuel elements are often unknown. To investigate the impact of the random distribution of positions and sizes of TRISO particles within a cuboid or cylindrical matrix on the temperature distribution of fuel elements and to establish a practical heat conduction model, TRISO fuel particles with randomly distributed positions, diameters following Gaussian or uniform distributions are generated using relevant algorithms. A cuboid and a cylindrical TRISO fuel element are modeled in ANSYS, and a three-dimensional temperature field distribution of the fuel element is obtained through numerical simulation. The probability density of the maximum temperature of the fuel element is calculated and fitted. Finally, the applicability of the two-regime heat conduction model over a broader range is validated based on the simulated data. The conclusions of this study provide reference information for predicting the temperature distribution of FCM fuel elements containing TRISO particles with random size and location distribution.

1. Introduction

1.1. Background

In today's advanced nuclear reactors, the application of fully ceramic microencapsulated (FCM) fuel, which comprises tri-structural isotropic (TRISO) fuel particles, has become widespread. A TRISO fuel particle consists of layers, progressing from the innermost to the outermost layers, including a fuel kernel, a porous carbon buffer layer, an inner dense pyrolytic carbon layer (IPyC), a silicon carbide layer (SiC), and an outer dense pyrolytic carbon layer (OPyC) (Demkowicz et al., 2019; Powers and Wirth, 2010). These particles can be dispersed within a graphite or silicon carbide matrix, forming the FCM nuclear fuel element. FCM fuel is classified as accident tolerant fuel (ATF) (Powers et al., 2013) and boasts excellent thermal performance and burnup characteristics (Petti et al., 2003). Its capacity to operate at higher temperatures and achieve greater burnup aligns well with the demands of modern reactors, especially high-temperature gas-cooled reactors (HGTR) (Li et al., 2021). Notably, it has been used in China's

experimental reactor, HTR-10 (Fang and Di Fulvio, 2023).

Owing to the unique manufacturing process, it is approximated that the fuel particles are randomly distributed within the matrix (Ji et al., 2014). Furthermore, during actual reactor operation, determining the size of TRISO fuel particles is also challenging. The precise size values or specific distribution details are often unknown, and typically, only a relatively broad range of size values can be obtained (Burke et al., 2012). This randomness and uncertainty present significant challenges when calculating the temperature field for dispersed TRISO nuclear fuel particles and in developing general models. To address the growing demand, it is necessary to propose a heat conduction model for TRISO-based FCM fuel elements, where TRISO fuel particles are dispersed randomly within a cuboid or cylindrical matrix, following various random size distributions. This will facilitate the practical application of this type of fuel in real reactors. This study, starting from the random distribution of fuel particles, employs simulation modeling to analyze and propose a simplified heat conduction model, laying the foundation for future studies.

* Corresponding author.

E-mail address: maolongliu@fudan.edu.cn (M. Liu).

Nomenclature		Greek symbols
k_e	effective thermal conductivity, W/(m·K)	Φ packing fraction of TRISO particles
k_p	equivalent thermal conductivity of particles, W/(m·K)	M mean value
k_m	equivalent thermal conductivity of matrix, W/(m·K)	Σ standard deviation
k_1	effective thermal conductivity of the inner region, W/(m·K)	B variable defined in equation (3)
D	particle diameter, m	K variable defined in equation (3)
A	Cuboid base side length, m	subscripts
R	cylinder radius, m	E effective
R_1	characteristic size of inner region, m	P particle
T	temperature, °C	M matrix
T_{out}	boundary temperature, °C	\max maximum
T_{in}	inner boundary temperature of annular matrix, °C	G Gaussian
T_{max}	maximum temperature, °C	U uniform
q''	volumetric heat power of particles, W/m ³	1 inner region

1.2. Previous studies

For FCM fuel elements with internally randomly dispersed TRISO particles, obtaining their effective thermal conductivity would allow predicting the temperature distribution within the fuel element by treating the fuel element as a uniform heat source. This is of significant importance for FCM fuel design and manufacturing. To calculate the effective thermal conductivity of composite materials, there are currently computational models based on Effective Medium Theories (EMT). Among these models, the Maxwell model and its derivatives, such as the Reduced Maxwell model, are representative (Maxwell, 1873). Their relationships can be expressed by Eqs. (1) and (2).

$$\frac{k_e}{k_m} = \frac{1 + 2\beta\phi}{1 - \beta\phi} \quad (1)$$

$$\frac{k_e}{k_m} = \frac{1 + \beta\phi}{1 - 0.5\beta\phi} \quad (2)$$

$$\beta = \frac{\kappa - 1}{\kappa + 2}, \kappa = \frac{k_p}{k_m} \quad (3)$$

where k_p and k_m are the equivalent thermal conductivity of particles and matrix, Φ is the packing fraction of particles. The Maxwell model assumes no thermal interaction between particles and is not suitable for predicting thermal conductivity at high packing fractions (Pietrak and Wiśniewski, 2015). Therefore, other researchers have modified the Maxwell model. For example, Chiew and Glandt (1983) proposed an improved effective thermal conductivity model that takes interactions between particles into account. Its form is shown in Eq. (4).

$$\frac{k_e}{k_m} = \frac{1 + 2\beta\phi + (2\beta^3 - 0.1\beta)\phi^2 + 0.05\phi^3 e^{4.5\beta}}{1 - \beta\phi} \quad (4)$$

Bruggeman (1935), on the other hand, altered the assumptions of the Maxwell model and did not distinguish between particles and the matrix. The Bruggeman model is shown in Eqs. (5) and (6).

$$\frac{k_e}{k_m} = \kappa A + (\kappa^2 A^2 + 0.5\kappa)^{0.5} \quad (5)$$

$$A = 0.25(3\phi - 1 + \frac{2 - 3\phi}{\kappa}) \quad (6)$$

Previous studies (Liu et al., 2018; Liu et al., 2019) conducted numerical simulations on cylindrical and spherical matrices with packing fractions not exceeding 50 %. The corresponding “two-regime” heat conduction model was introduced, which treats the entire matrix as two distinct regions. The inner region is formed by TRISO fuel particles

mixed with the matrix in the densest packing. The remaining portion of the original matrix constitutes the outer region, composed of the matrix material. This model excels in predicting the highest temperature for TRISO-based FCM fuel elements.

Furthermore, some researchers have investigated the random distribution and heat conduction performance of spherical fuel particles in a cylindrical or spherical matrix. Folsom et al. (2015) carried out experimental and numerical simulations on the effective thermal conductivity (ETC) of TRISO fuel particles, obtaining that the Chiew and Glandt model provides more accurate predictions for the ETC of this type of fuel. The research revealed that due to the influence of composite materials on the anisotropy of the matrix material, it is advisable to directly measure the effective thermal conductivity of composite materials rather than measuring the thermal conductivities of the matrix and particles separately to obtain more accurate ETC values. Zhang et al. (2023) employed an irradiation-thermo-mechanical coupling method and optimization techniques to find the optimal parameters for TRISO-based FCM fuel elements, considering material properties, fuel geometry, and particle arrangement. Gong et al. (2023) used COMSOL to study the effective thermal conductivity of FCM fuel elements with randomly embedded multilayer TRISO particles. They established a three-dimensional heat conduction model based on the Finite Element Method (FEM) for the random distribution of TRISO particles and found that the ETC of FCM fuel with randomly embedded fuel particles follows a Gaussian distribution. Wang et al. (2023a,b) introduced multi-scale heat conduction models for the random distribution of TRISO particles, including Multi-region Layered (ML), Multi-region Non-layered (MN), Homogeneous, and Multi-annulus models. The study revealed that the Homogeneous model with internal heat sources and the Multi-annulus model can accurately predict the average temperature of FCM fuel elements at different packing fractions and the maximum temperature of fuel elements at higher loadings.

Burke et al. (2012) found that the size of TRISO fuel particles is not constant but follows random distribution patterns, including both Gaussian and uniform distributions. To date, no researchers have specifically investigated the heat conduction models for cylindrical or cuboid FCM fuel elements with randomly distributed sizes of TRISO particles. Hence, numerical simulations are utilized to explore the temperature field under scenarios where nuclear fuel sizes and positions are randomly distributed and a corresponding heat conduction model is established.

It is worth noting that the transient performance of FCM fuel elements has a significant impact on reactor design and safety analysis (Brown, 2020). Some integral fuel safety tests conducted in experimental reactors (IAEA, 1997; Umeda et al., 2010; Fukuda et al., 1990) have investigated the relationship between energy deposition and

failure rates of TRISO-based FCM fuel applied to High-Temperature Gas-cooled Reactors (HTGRs). The Transient Reactor Test Facility (TREAT) at the Idaho National Laboratory (INL) has also conducted experimental validations which may be helpful for advanced TRISO fuel concepts proposed for light-water reactors (Woolstenhulme et al., 2020; Hernandez et al., 2020), thereby filling in data gaps.

Also, past works have extensively studied the impact of different thermal properties homogenization of FCM fuel, including effective thermal conductivity, on the transient behavior of reactors. Brown et al. (2013) evaluated the reactivity insertion transients of FCM-fueled Pressurized Water Reactors (PWRs) under different rod insertion conditions, considering different homogenization treatments for FCM fuel and burnable poison configurations at the beginning and end of the cycle. They found that the reactivity insertion transients were highly sensitive to the thermal homogenization of FCM fuel. Lee and Cho (2015, 2016, 2014) homogenized the matrix and TRISO particles and solved the heat conduction equation separately. They proposed a two-temperature homogenized thermal conductivity model using the particle transport Monte Carlo method and coupled it with a neutron diffusion model. This approach provided temperature-based homogenization parameters such as thermal conductivity and volumetric heat capacity. They analyzed the steady-state performance and transient response of FCM fuel-loaded cores and found that their proposed model could provide more realistic temperature results compared to traditional models, thus better predicting Doppler temperature feedback.

In conducting steady-state analyses, thermal conductivity is considered the key thermal property in this study. The two-regime model is used to assess the steady-state thermal performance of TRISO particles with random size and position distributions. However, it is found that volumetric heat capacity is far more important than thermal conductivity in transient response (Lee and Cho, 2015). It affects the rate of temperature change in FCM fuel elements and thereby influences the Doppler temperature feedback. This aspect is not covered in this paper and further studies are needed to provide transient analyses of reactor performance and safety characteristics of TRISO fuel.

2. Numerical simulation

2.1. The algorithm for random generation

A combination of a “neighbor-based generation algorithm” and a conventional random algorithm is used for the random generation of fuel particles. The conventional random algorithm randomly generates

the coordinates and radius of each particle. After the generation, it checks whether the particle overlaps with other existing particles. If there is an overlap, it regenerates the particle until there is no overlap. This method exhibits strong randomness but has lower efficiency in generating fuel particles at high packing fractions.

To enhance the utilization efficiency of matrix voids at high packing fractions, the “neighbor-based generation algorithm” is introduced. Firstly, this algorithm randomly selects an already generated particle and uses the Marsaglia method (Marsaglia and Bray, 1964) to search for non-overlapping regions on a spherical surface concentric with the selected particle and a radius equal to the sum of the radius of the selected particle and the radius of the particle to be generated. If no suitable location is found, it repeats the process by selecting another already generated particle until a fillable position is located. This method maintains a certain level of randomness while improving the efficiency of particle generation at high packing fractions, reducing the time and cost involved in random generation modeling. The specific process for obtaining the center coordinates of the required fuel particles is outlined in Fig. 1. In scenarios with a high packing fraction, the first 5 % of the fuel particles are randomly generated using a standard random algorithm. And for the remaining ones, the neighbor-based generation algorithm is employed.

In addition, for the random distribution of particle diameters, considering diameter d_g to follow a Gaussian distribution within $[d - \Delta d, d + \Delta d]$, based on the principles of rare events and hypothesis testing, it can be assumed that $d_g \sim N(d, (\Delta d)^2/9)$. For diameter d_u taking on values within $[d - \Delta d, d + \Delta d]$ and following a uniform distribution $U(d - \Delta d, d + \Delta d)$, it can be represented by equation (7), where δ is a random number in the range between 0 and 1. Additionally, contrasting with the two random distributions, cases with constant diameter are set up.

$$d_u = d + 2\Delta d(\delta - 0.5) \quad (7)$$

2.2. Geometry and mesh

This research utilizes ANSYS software for detailed modeling. The specific modeling and simulating approach involves using the steady-state thermal module within the software. In the selection of the size parameters for the cuboid and cylindrical matrix, it is ensured that the volumes of the two types of matrices are relatively close, while parameters that are more suitable for random generation process are chosen. Fig. 2 shows the mesh generation on the matrix and particles when the mesh size is 0.1 mm at the highest packing fraction. Additionally, in

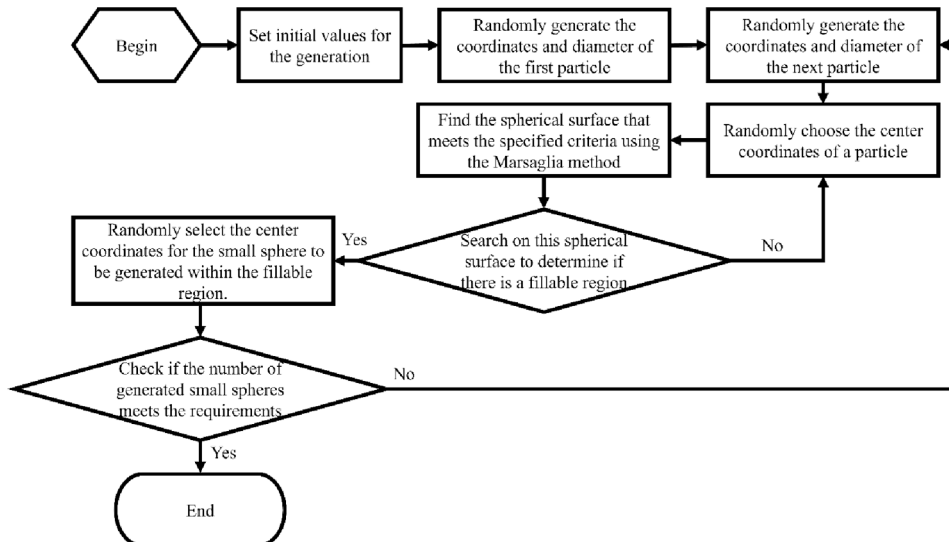


Fig. 1. Flowchart of neighbor-based generation algorithm.

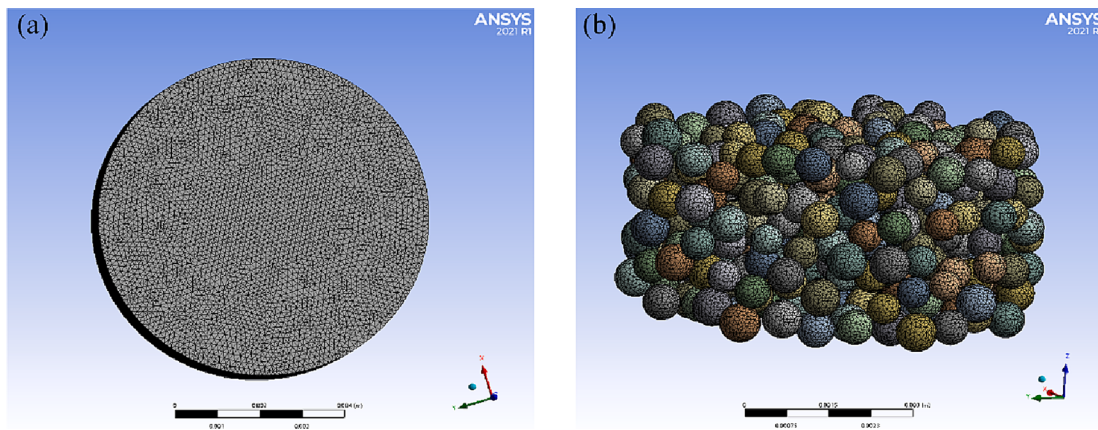


Fig. 2. Mesh: (a) Matrix, (b) Particles.

reference to the previous studies (Liu et al., 2018; Liu et al., 2019), and considering the complexity of modeling, a simplification and equivalence approach using uniform material is applied to the multi-layer TRISO fuel particles. For modeling, graphite is used for the matrix material. The parameters for the modeled fuel element and particle sizes are listed in Table 1 and Table 2.

2.3. Boundary conditions

In the calculations, ideal adiabatic boundary conditions are applied to the top and bottom surfaces of the cuboid and cylindrical matrices, while isothermal boundary conditions are applied to the lateral surfaces. The boundary temperature is set to 800 °C, and internal heat source boundary conditions are applied to all fuel particles with a parameter set to 10⁹ W/m³. This value is used as the heat generation rate of TRISO particles for all cases in this study and is calculated by equation (8), where the linear power and packing fraction are 200 W/cm and 0.42 (Terrani et al., 2012), respectively. A schematic diagram of the boundary conditions can be seen in Fig. 3.

$$q' = \frac{qH}{\phi V_{matrix}} \quad (8)$$

Where q' is the linear power, H is the height of cylindrical matrix, ϕ is the packing fraction and V_{matrix} is the volume of cylindrical matrix.

2.4. Mesh independency

Mesh independence analysis is conducted using the highest packing fraction as the analysis condition. The variation of the maximum temperature with mesh size can be seen in Fig. 4. The numerical simulation results for the maximum temperature remain approximately constant at a mesh size of around 0.1 mm. Considering that excessively small mesh sizes would incur additional computational costs, a final mesh size of 0.1 mm is selected.

2.5. Model validation

To validate the reliability of the numerical model, the results of

Table 1
Geometric model parameters.

Geometric parameters	Value (mm)
Cylinder radius	3.9
Cylinder height	3.9
Cuboid base side length	6.3
Cuboid height	5.0

Table 2
Simulation parameters.

Parameters	Value
Matrix Thermal Conductivity [W/(m·K)]	25
TRISO particle equivalent thermal conductivity [W/(m·K)]	3.77
TRISO Particle radius (mm)	0.29 ~ 0.37
Packing fraction	0.1 ~ 0.3

calculations under different packing fractions with a uniform or Gaussian diameter distribution are compared with the Maxwell model and its derivative models (eq. (1)-(6)). Taking the cylindrical matrix as an example, Fig. 5 shows the comparison of the model estimated values and simulated values for the maximum temperature and the average temperature of the matrix.

As shown in Fig. 5, the numerical model established in the study matches well with the results of the Maxwell model, with maximum errors in maximum temperature and average temperature not exceeding 4 % and 2 %, respectively. For cases with lower packing fractions, the model consistently adheres to the underlying assumptions of the Maxwell model, resulting in relatively modest deviations from its calculated results. Nevertheless, as the packing fractions increase, the interparticle interactions become more prominent, leading to a gradual departure of the simulated values from the calculations provided by the Maxwell model. In summary, the numerical model established in this study underscores its reliability by its alignment with the results of pertinent models.

2.6. Simulation scenarios

The study carries out numerical simulations for 60 different scenarios, each with Gaussian size distribution, uniform size distribution or constant particle size, all within packing fractions ranging from 10 % to 30 %, using the thermal boundary conditions described in section 2.3. The specific conditions are detailed in Table 3. Due to the adiabatic conditions at the top and bottom surfaces and the overall geometric symmetry, a cross-section through the center of the cylindrical and cuboid base is chosen as the characteristic plane. Several temperature calculation paths are set at regular intervals on this cross-section. A schematic diagram can be seen in Fig. 6.

3. Results

3.1. Temperature distribution

The temperature field calculation results that include the entire cuboid matrix, cylindrical matrix, and TRISO fuel particles are obtained.

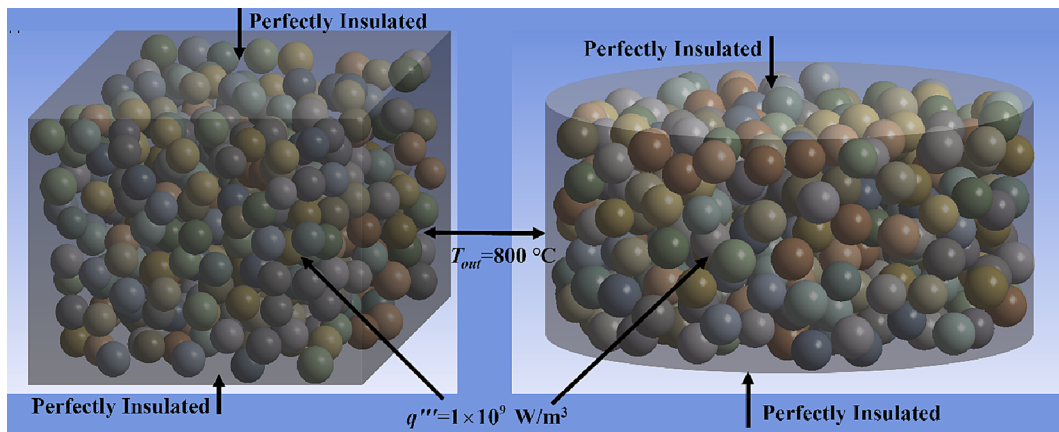


Fig. 3. Boundary condition.

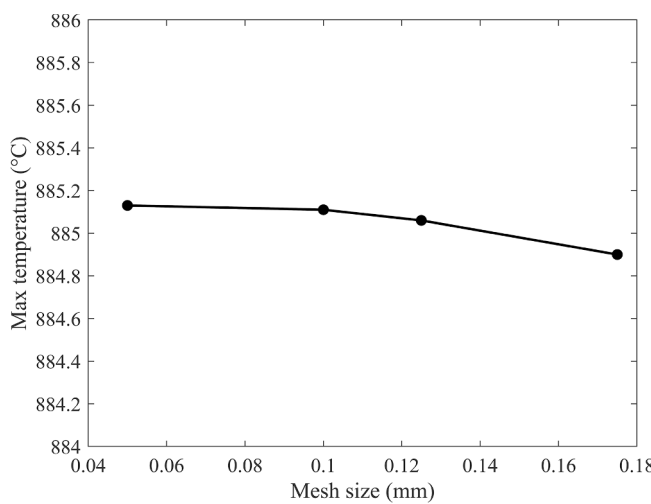


Fig. 4. Fuel element maximum temperature under different mesh sizes.

Fig. 7 depict the temperature field calculation results for a specific case with a Gaussian diameter distribution at packing fraction $\phi = 30\%$. The figures show that both the cuboid and cylindrical bases have the highest temperature at the center region, forming a hot region.

3.2. Maximum temperature

Fig. 8 illustrates statistical information of the maximum temperature probability histogram, taking the results at a packing fraction of 20% as an example. And the probability density fitting curves for the maximum temperature of three packing fractions are shown in Fig. 9. Fig. 8 and Fig. 9 reveals that the distribution of the maximum temperature can be considered as a Gaussian distribution.

The mean value of the maximum temperature reflects its overall level. The increase in packing fraction results in a higher equivalent volumetric heat power among matrix and particles, gradually raising the mean value of the maximum temperature. Also, according to the contours from Section 3.1, it can be observed that the maximum temperature of the FCM fuel elements occurs in the central hot region. The random distribution of particle size influences the position of particles in the central region, which affects the mean value of the maximum temperature. Comparing cases following Gaussian and uniform distribution, the temperature results for both cases show small differences. However, comparing the cases of random size distribution and the case of constant size, it can be obtained that with consistent mean particle sizes, for the cylindrical matrix, random size distribution has a certain impact on the

mean value of the highest temperatures, increasing the maximum temperature of the FCM fuel element by approximately 5 °C at most. But for the cuboid matrix, this impact is less pronounced.

The standard deviation of the highest temperature reflects the influence of randomness under different conditions. This influence varies in the entire matrix and the central hot region. From the perspective of the entire region, with increasing packing fraction, although the spatial positions of the fuel particles become more certain, leading to a decreasing standard deviation, the fact that the diameters of fuel particles also follow a Gaussian or uniform distribution leads to a potential increase in the variability, resulting in an increasing standard deviation.

In the central hot region, the effect of particle size random distribution coupled with the increase in the number of fuel particles leads to a more complex arrangement of fuel-to-matrix relative positions. Different sized particles introduce varying packing patterns, thereby altering the local packing fraction within the central hot region and consequently affecting the standard deviation of the highest temperature.

As the packing fraction increases, the standard deviation of the simulated peak temperature either decreases first and then increases or consistently increases. The specific trend is closely related to the shape of the matrix and the random distribution pattern of particle diameters. Comparing the three sets of simulation results, the standard deviation of the maximum temperatures for the various conditions of the two types of matrices decreases in the following order: uniform size distribution, constant size, and Gaussian size distribution.

4. The two-regime model

4.1. Model development

In section 1.2, a preliminary introduction to the basic idea of the two-regime model is provided. Considering that this model is established based on the condition where equally sized TRISO fuel particles are randomly dispersed in cylindrical or spherical matrices, the two-regime model is validated by incorporating numerical simulation results considering the random distribution of TRISO particle sizes and their dispersion in matrices of various shapes.

The two-regime model (Liu et al., 2019) equates the entire matrix to two regions, with the inner and outer region conceptually illustrated as if the TRISO particles are “compressed” inward, as shown in Fig. 10(a)-(d). The inner region is formed by TRISO fuel particles mixed with the matrix through the densest packing, sharing the same height as the original matrix and a cross-sectional shape that is proportionally reduced. The remaining portion of the original matrix constitutes the outer region, composed of the same material as the matrix. The radial temperature distribution at the central cross-section is obtained by

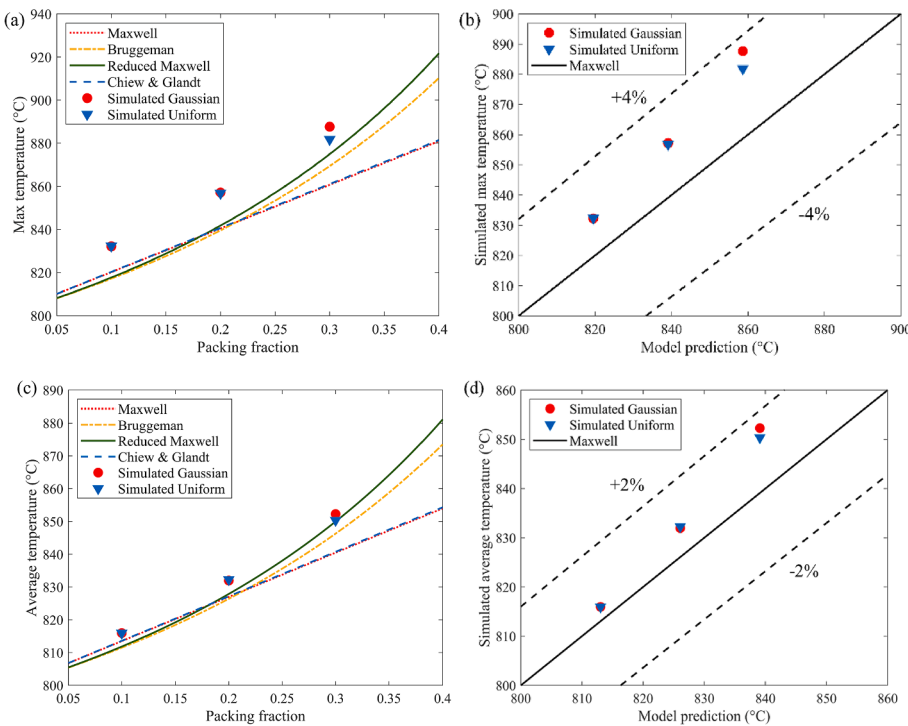


Fig. 5. Comparison of simulated and model estimates of matrix temperature: (a) Maximum temperature, (b) Relative error of maximum temperature, (c) Average temperature, (d) Relative error of average temperature.

Table 3
Parameters of the simulation scenarios.

Parameters	Value
Particle radius distribution	Gaussian distribution
Packing fraction (%)	10 %, 20 %, 30 %
Number of scenarios for each packing fraction	60

solving the one-dimensional steady-state heat conduction equation in cylindrical and spherical coordinates, as indicated by Eqs. (9) and (10). The volumetric heat power in the inner region is equivalently modeled using uniform heat generation, while the thermal conductivity is equivalently determined using the results of the Maxwell model calculations at the original packing fraction, as expressed in Eqs. (11) and (12).

$$k_1 \nabla^2 T + q''_1 = 0, \text{ for inner region} \quad (9)$$

$$k_m \nabla^2 T = 0, \text{ for outer region} \quad (10)$$

$$q''_1 = \phi_{max} q''' \quad (11)$$

$$k_1 = \frac{1 + 2\beta\phi}{1 - \beta\phi} k_m \quad (12)$$

For the cuboid matrix with a square base, considering symmetry, the temperature distribution along the x-axis direction is examined. Since the solution only involves the one-dimensional heat conduction equation along the x-axis, the particles should be “compressed” only along the x-axis to form inner and outer regions, as illustrated in Fig. 10(c).

Furthermore, applying the two-regime model for cylindrical matrices to an annular matrix, the partitioning can be obtained as shown in Fig. 10(d). It should be noted that for the annular matrix, isothermal boundary conditions are applied to both its inner and outer cylindrical

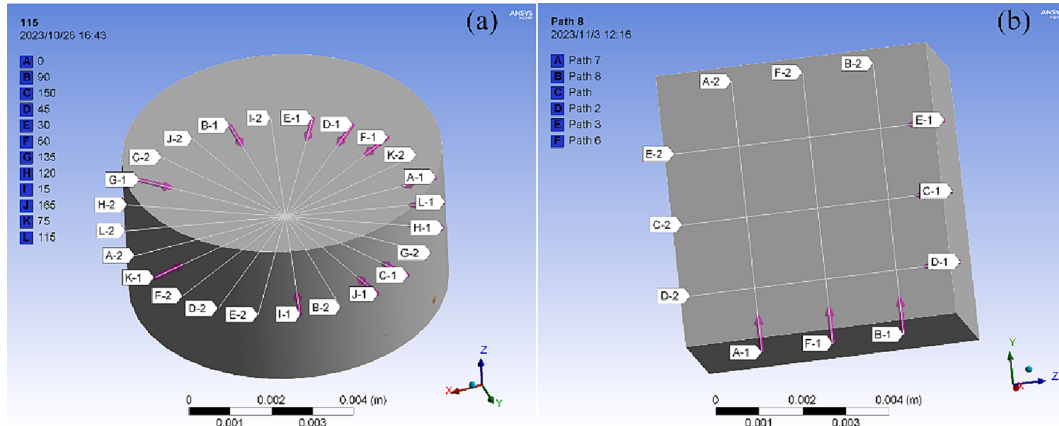


Fig. 6. Characteristic lines: (a) Cylindrical matrix, (b) Cuboid matrix.

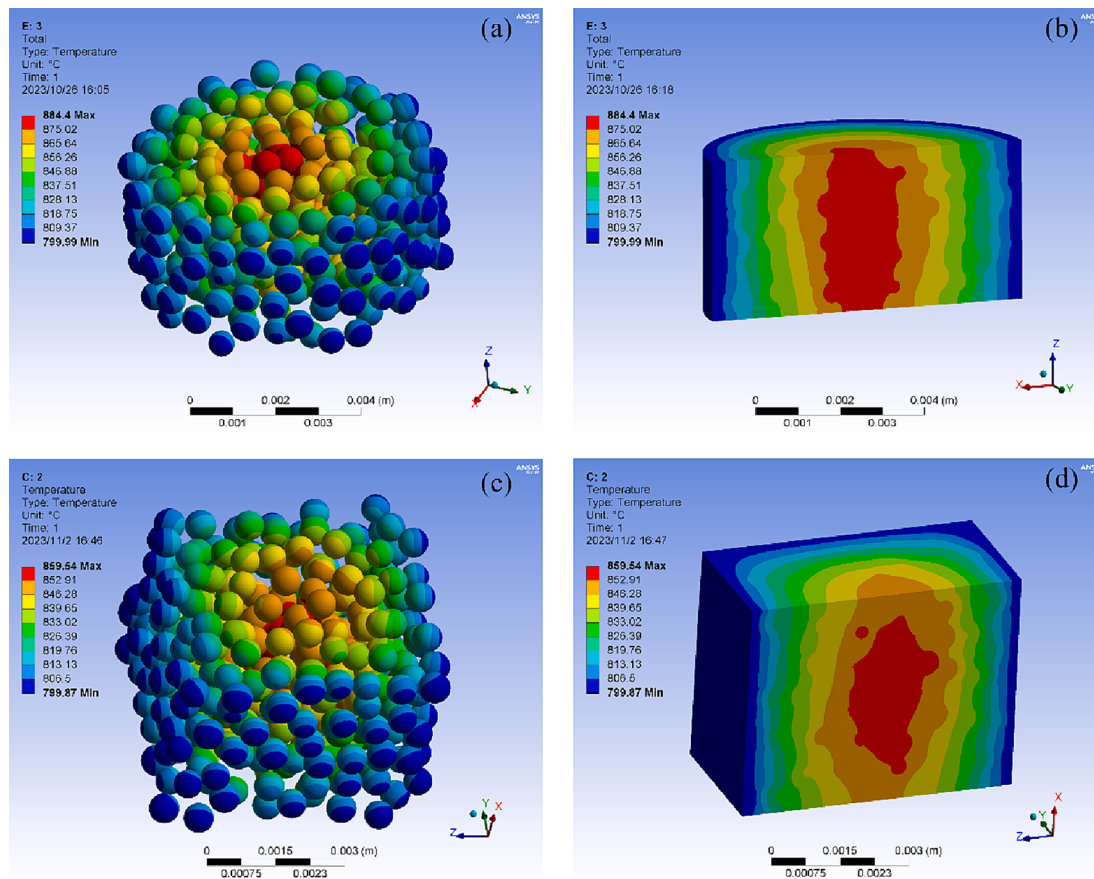


Fig. 7. Temperature contours ($\phi = 30\%$): (a)-(b) Cylindrical matrix; (c)-(d) Cuboid matrix.

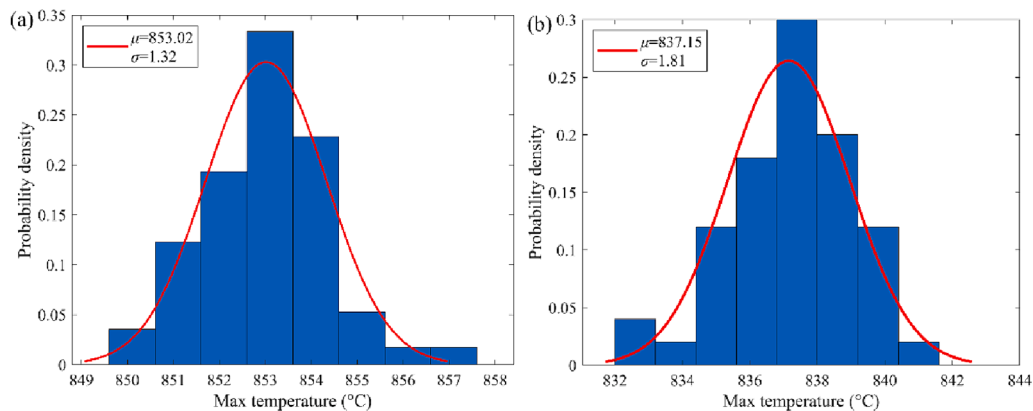


Fig. 8. Statistical distribution of the maximum temperature ($\phi = 20\%$): (a) Cylindrical matrix, Gaussian size distribution; (b) Cuboid matrix, uniform size distribution.

surfaces, with temperatures denoted as T_{in} and T_{out} , respectively. The characteristic size of the inner region and numerical solutions of the temperature field for various matrices in the upgraded two-regime model are presented in Table 4.

4.2. Model validation

Taking the scenario of the cylindrical matrix, uniform particle diameter distribution, and a packing fraction of 10 % as an example, Fig. 11 illustrates the temperature distribution along the calculation paths described in section 2.6 under all 60 random distribution conditions. The purple shaded area represents the region enclosed by the

upper and lower envelope lines of the radial temperature distribution along all calculation paths. Due to the random distribution of particle positions and sizes, the temperature distribution results differ among different conditions and calculation paths. Hence, the shaded area is used to represent the possible range of values for the radial temperature distribution at the mid-section.

The temperature distribution results are depicted in Fig. 12 and Fig. 13 using the shading approach as shown in Fig. 11, compared to the model results introduced in section 4.1. Compared to constant particle size, the random size distribution makes the packing of TRISO particles in the matrix more diverse. Depending on the size of particles participating in packing and the geometric structure of the matrix, there may

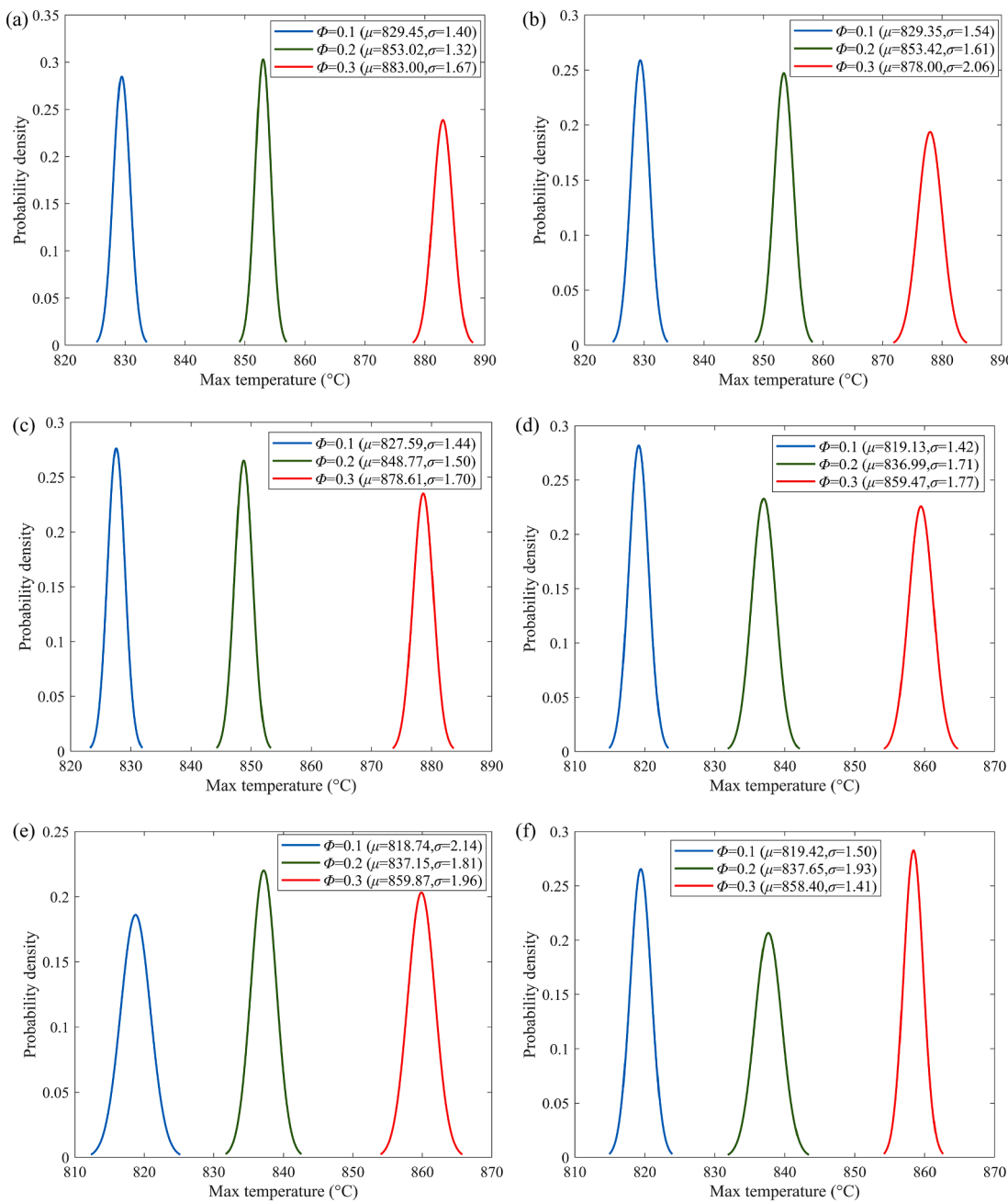


Fig. 9. Distribution of the maximum temperature: (a) Cylindrical matrix, Gaussian size distribution; (b) Cylindrical matrix, uniform size distribution; (c) Cylindrical matrix, constant size; (d) Cuboid matrix, Gaussian size distribution; (e) Cuboid matrix, uniform size distribution; (f) Cuboid matrix, constant size.

be a more compact or more dispersed packing, resulting in an overall increase or decrease in temperature level. It can be observed that an increase in packing fraction, on one hand, leads to a more diverse distribution of random sizes, facilitating the diversity of packing. On the other hand, it also reduces the available “voids” for packing in the matrix, limiting the diversity of packing. These combined effects result in changes in temperature distribution due to variations in matrix geometry, random particle size distribution, and packing fraction.

Fig. 12 shows the results of cases with the cylindrical matrix. Due to its relatively flat shape, particles tend to exhibit compact packing, which leads to a higher temperature level for both Gaussian and uniform particle size distributions compared to the case with constant particle size. At a 30 % packing fraction, the restriction on packing “voids” results in less diverse packing patterns. The case with more extreme sizes, following uniform distribution, is more sensitive to this effect,

potentially leading to relatively discrete packing patterns, gradually converging towards the results of the case with constant size. Conversely, the case with Gaussian distribution, with fewer extreme sizes, still maintains a temperature difference of approximately 5 °C compared to the constant particle size condition.

Fig. 13 depicts the results of cases with the cuboid matrix, which has relatively balanced axial and radial dimensions. Particles exhibit both compact and dispersed packing patterns, leading to a mutual balance, which results in the temperature distribution of cases with random size distribution at various packing fractions being closer to that of cases with constant size.

Compared to the model results, for both simulated matrices, as the packing fraction of TRISO particles increases, it gradually approaches the most densely packed fraction, and the simulation results also progressively converge with the model results. Furthermore, as the two-

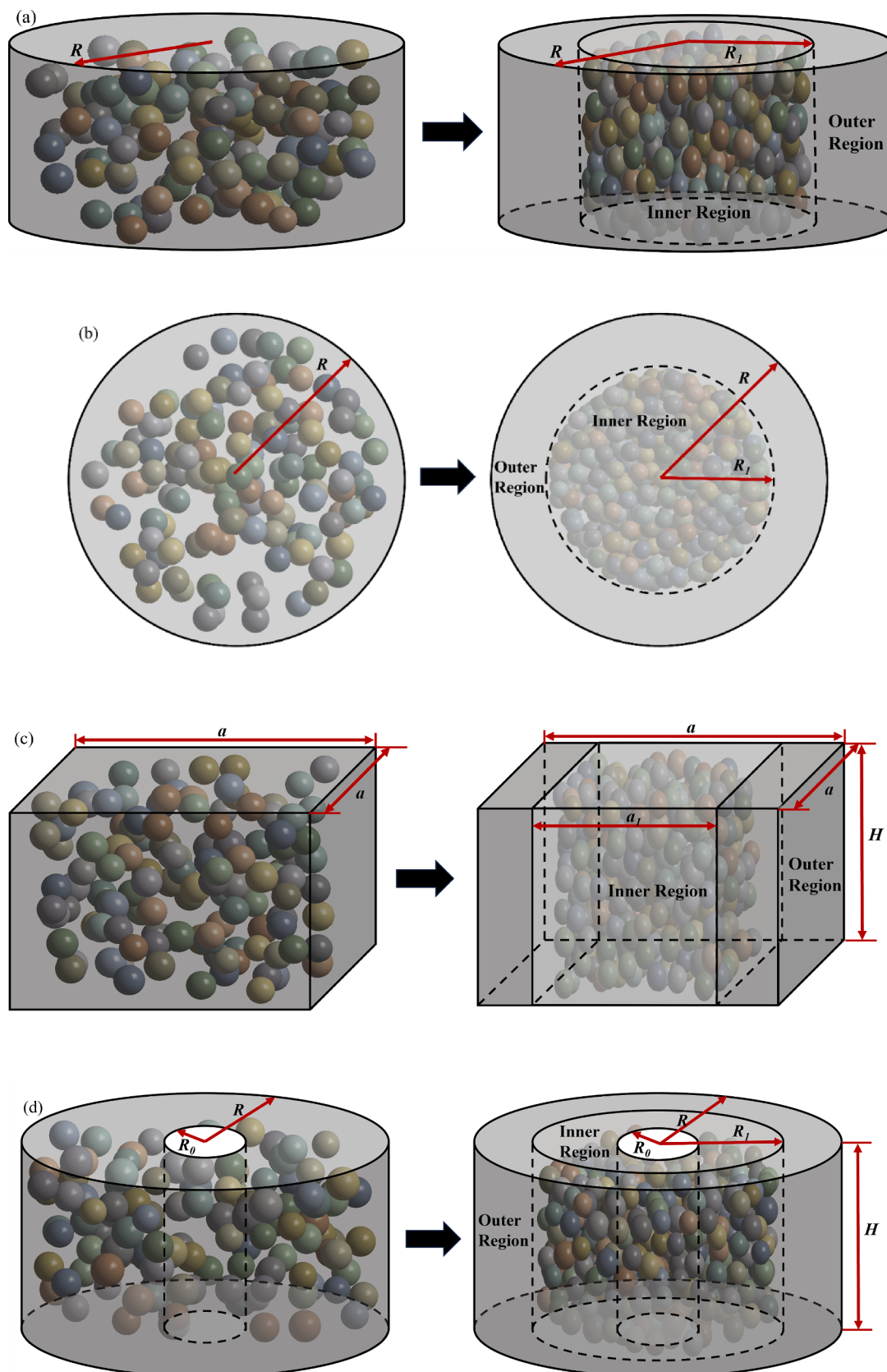
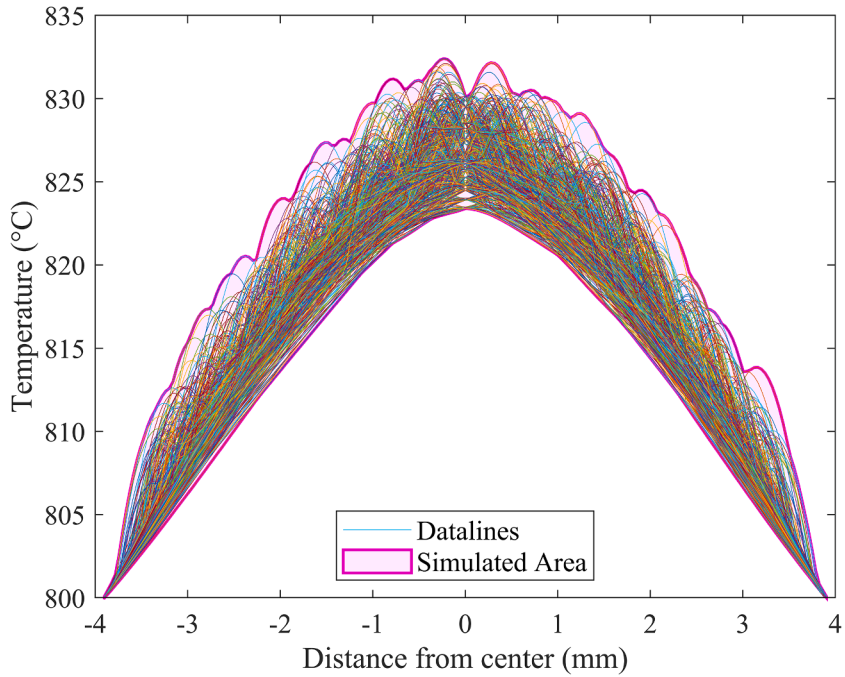


Fig. 10. Schematic diagram of the two-regime model: (a) Cylindrical matrix, (b) Spherical matrix, (c) Cuboid matrix, (d) Annular matrix.

Table 4

The two-regime model: characteristic size and temperature distribution for various matrices.

Shape of the matrix	Characteristic size of the inner region	Temperature distribution
Cylinder	$R_1 = \sqrt{\frac{\phi}{\phi_{max}} R}$	$T = \begin{cases} \frac{q''_1 R_1^2}{2k_m} \ln\left(\frac{R}{R_1}\right) + \frac{q''_1}{4k_1} (R_1^2 - r^2) + T_{out}, & 0 \leq r \leq R_1 \\ \frac{q''_1 R_1^2}{2k_m} \ln\left(\frac{R}{r}\right) + T_{out}, & R_1 \leq r \leq R \end{cases}$
Sphere	$R_1 = \sqrt[3]{\frac{\phi}{\phi_{max}} R}$	$T = \begin{cases} \frac{q''_1 R_1^3}{3k_m} \left(\frac{1}{R_1} - \frac{1}{R}\right) + \frac{q''_1}{6k_1} (R_1^2 - r^2) + T_{out}, & R_0 \leq r \leq R_1 \\ \frac{q''_1 R_1^3}{3k_m} \left(\frac{1}{r} - \frac{1}{R}\right) + T_{out}, & R_1 \leq r \leq R \end{cases}$
Cube	$a_1 = \frac{\phi}{\phi_{max}} a$	$T = \begin{cases} -\frac{q}{2k_1} (x^2 - \frac{a_1^2}{4}) + \frac{qa_1}{4k_m} (a - a_1) + T_{out}, & 0 \leq x \leq a_1 \\ -\frac{qa_1}{2k_m} (x - \frac{a}{2}) + T_{out}, & a_1 \leq x \leq \frac{a}{2} \end{cases}$
Annulus	$R_1 = \sqrt{\frac{V_p}{\pi H \phi_{max}} + R_0^2}$	$T = \begin{cases} -\frac{q''_1}{4k_1} (r^2 - R_0^2) + C_a k_m \ln \frac{r}{R_0} + T_{in}, & R_0 \leq r \leq R_1 \\ (-\frac{q''_1 R_1^2}{2k_m} + C_a) \ln \frac{r}{R} + T_{out}, & R_1 \leq r \leq R \end{cases}$

**Fig. 11.** Schematic diagram of the shaded area.

regime model considers the outer region as matrix and the inner region as a mixture of matrix and particles under the densest packing, its temperature predictions are lower in the peripheral areas of the matrix than the simulated highest values, but higher in the central region.

For cuboid matrices, due to the two-regime model's sole resolution of one-dimensional steady-state heat conduction equations in a single direction, at low packing fractions, the results exhibit significant deviations from the actual conditions, leading to consistently elevated temperature field estimates compared to the simulations. In summary, within the scope of this study, for cylindrical and cuboid matrices, the two-regime model provides a relatively conservative prediction of the upper envelope of the radial temperature distribution in the central region after variations in the size of TRISO particles. Additionally, the applicability of the model to spherical matrices has been validated in previous studies. However, this paper does not include relevant validation results for annular matrices, and further study is needed.

5. Discussion

The accurate prediction of the maximum temperature in FCM fuel elements is crucial for safety analysis. Traditional research methods for this issue can generally be divided into two categories: one treats the matrix and TRISO particles as a whole, using the assumption of uniform heat generation to calculate the equivalent thermal conductivity for determining the maximum temperature; the other considers TRISO particles as radially uniform spherical heat sources randomly distributed in the matrix. Both methods are limited in reliably simulating the temperature distribution of TRISO particles with random sizes and positions dispersed in the matrix, which is commonly observed in practical applications.

Building upon the latter method, this study introduces a modification by assuming that the TRISO particle sizes follow either a Gaussian or a uniform distribution, making it more realistic. Additionally, this research extends and refines a two-regime heat conduction model developed in a previous study (Liu et al., 2019), which is applicable to

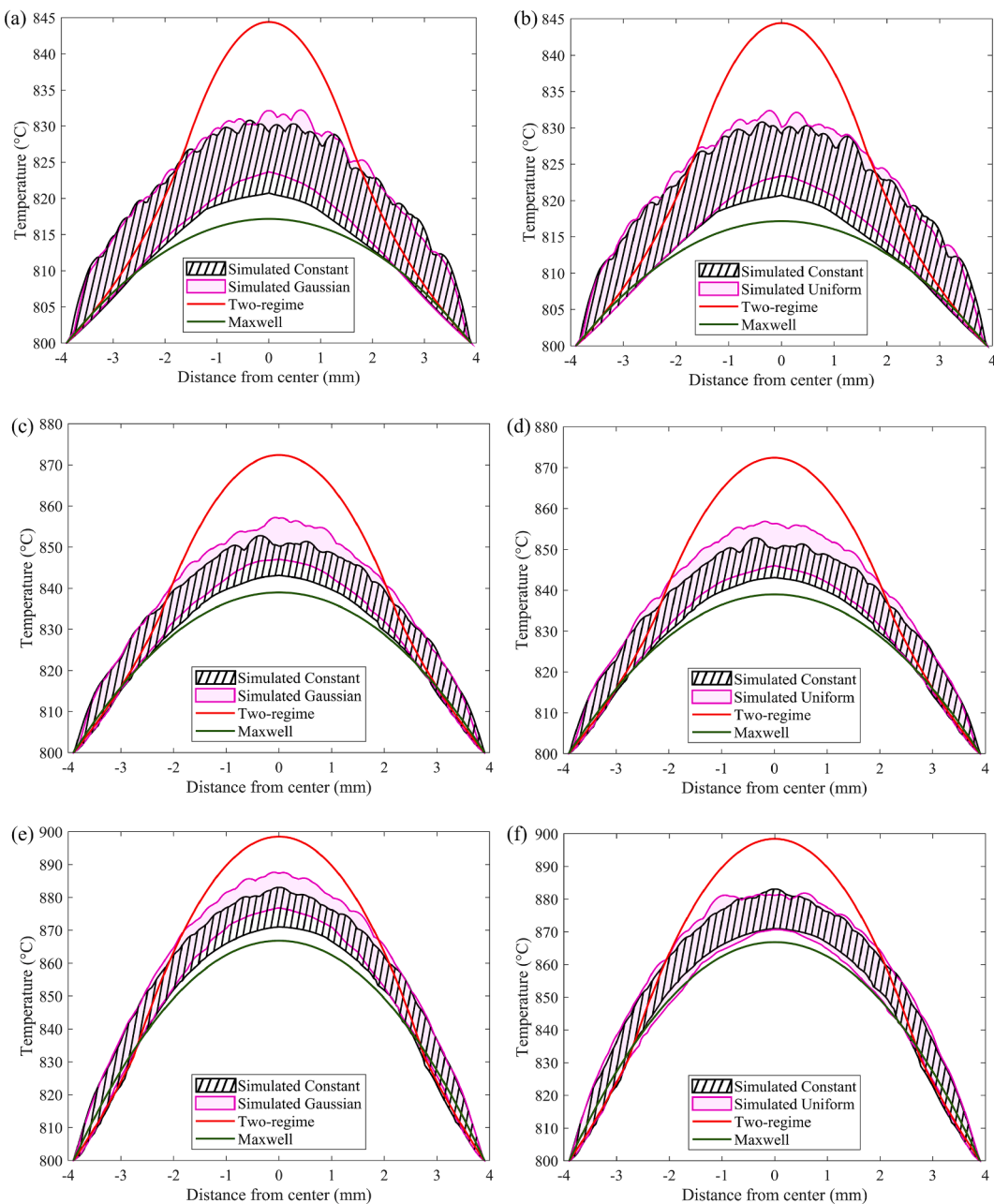


Fig. 12. Comparison of simulation results with model results for the cylindrical matrix: (a) $\Phi = 10\%$, constant versus Gaussian distribution; (b) $\Phi = 10\%$, constant versus uniform distribution; (c) $\Phi = 20\%$, constant versus Gaussian distribution; (d) $\Phi = 20\%$, constant versus uniform distribution; (e) $\Phi = 30\%$, constant versus Gaussian distribution; (f) $\Phi = 30\%$, constant versus uniform distribution.

spherical and cylindrical matrices under the assumption of uniform particle sizes, by accounting for different particle size distributions and diverse matrix shapes. The results indicate that, compared to traditional homogeneous models, the two-regime model can better predict the maximum temperature and temperature distribution in cylindrical and cuboid matrices under the mentioned conditions in a conservative way. This model is suitable for the preliminary safety analysis of TRISO-based FCM fuel elements.

Future research should include further validation studies on the applicability of the model to matrices with various shapes, such as spherical and annular matrices, after variations in particle size. Additionally, as burnup increases, elastic and thermal strains between different layers of TRISO fuel particles may lead to the formation of cracks (Haynes et al., 2023), introducing additional thermal resistance between the layers and affecting the accurate prediction of temperature.

Further numerical studies could be conducted by randomly selecting a certain proportion of TRISO fuel particles to acquire extra thermal resistance between different layers, in order to analyze the impact of the quantity of fuel particles with additional thermal resistance and the value of the thermal resistance on the maximum temperature of FCM fuel element, evaluating the uncertainties.

6. Conclusion

Numerical studies are conducted on the heat conduction model with randomly distributed TRISO fuel particles having random positions and sizes in both cuboid and cylindrical matrices. The main conclusions of this study are as follows:

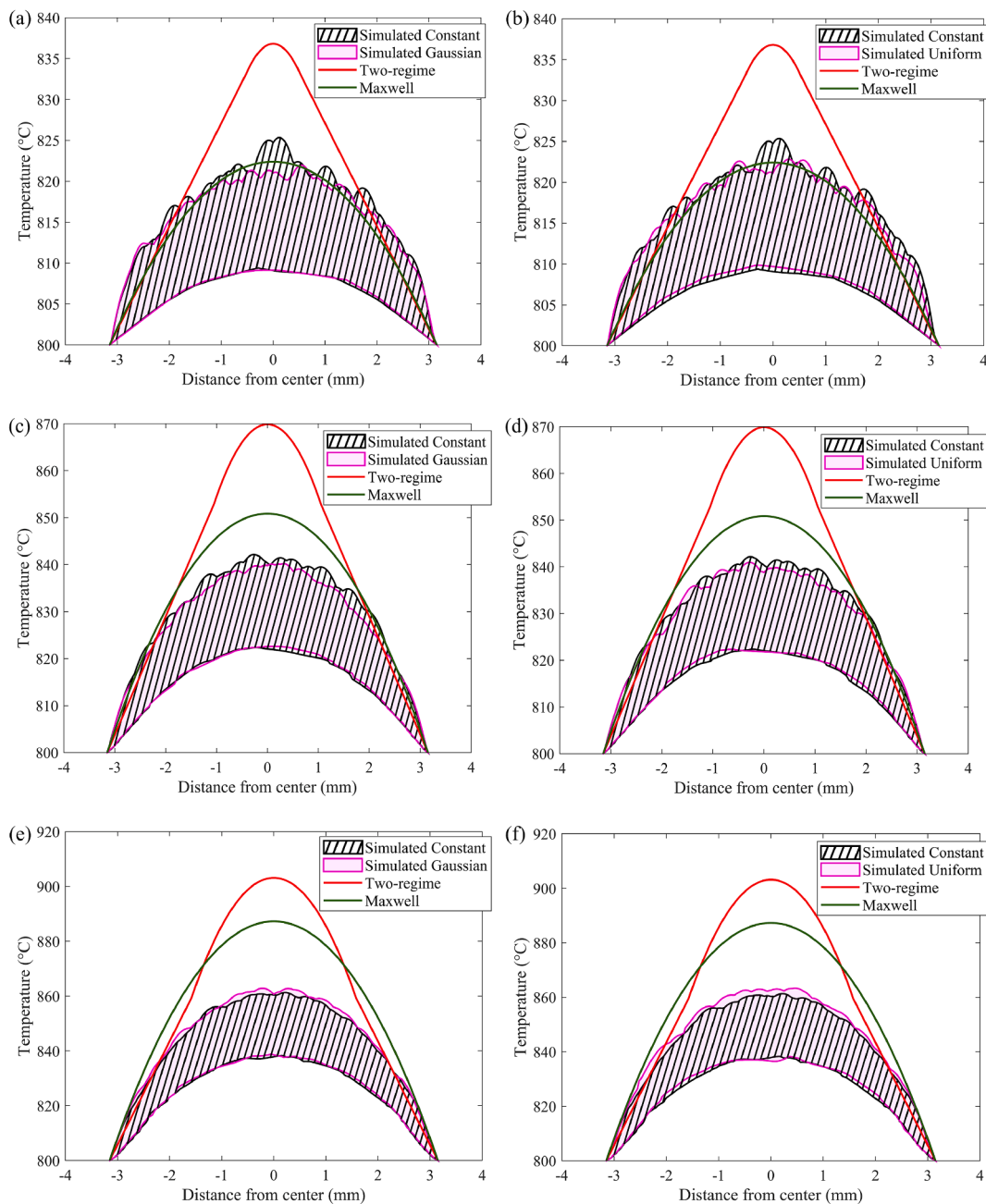


Fig. 13. Comparison of simulation results with model results for the cuboid matrix: (a) $\phi = 10\%$, constant versus Gaussian distribution; (b) $\phi = 10\%$, constant versus uniform distribution; (c) $\phi = 20\%$, constant versus Gaussian distribution; (d) $\phi = 20\%$, constant versus uniform distribution; (e) $\phi = 30\%$, constant versus Gaussian distribution; (f) $\phi = 30\%$, constant versus uniform distribution.

- (1) The combination of a conventional random algorithm and the “neighbor-based generation algorithm” allows for the generation of TRISO fuel particles with random positions in the matrices and with diameters following Gaussian or uniform distribution.
- (2) The numerical simulations yield three-dimensional temperature field distributions within the fuel elements. The results show that the simulation results of the maximum temperature in the fuel elements approximately follow a Gaussian distribution.
- (3) The random distribution of particle sizes has a certain impact on the temperature distribution of FCM fuel elements. For the cylindrical matrix, the temperature level for cases with Gaussian and uniform particle size distributions is higher compared to cases with constant particle size. Random size distributions increase the mean value of the maximum temperature of the FCM

fuel elements by approximately 5 °C at most. However, for the cuboid matrix, this effect is less pronounced.

- (4) The two-regime model performs admirably in predicting the upper envelope of radial temperature distribution for TRISO particles within cylindrical and cuboid matrices, after variations in particle size.

CRediT authorship contribution statement

Chunxi Wu: Writing – review & editing, Writing – original draft, Validation, Methodology, Investigation, Formal analysis, Data curation, Conceptualization. **Guitao Yang:** Validation, Methodology, Investigation, Data curation. **Wei Zhang:** Methodology, Investigation, Data curation. **Xianglong Guo:** Conceptualization. **Maolong Liu:** Writing –

review & editing, Supervision, Software, Resources, Conceptualization.

Declaration of competing interest

The authors declare that they have no known competing financial interests or personal relationships that could have appeared to influence the work reported in this paper.

Data availability

Data will be made available on request.

References

- Brown, N.R., 2020. A review of in-pile fuel safety tests of TRISO fuel forms and future testing opportunities in non-HTGR applications. *J. Nucl. Mater.* 534, 152139. <https://doi.org/10.1016/j.jnucmat.2020.152139>.
- Brown, N.R., Ludewig, H., Aronson, A., Raitses, G., Todosow, M., 2013. Neutronic evaluation of a PWR with fully ceramic microencapsulated fuel. Part II: nodal core calculations and preliminary study of thermal hydraulic feedback. *Ann. Nucl. Energy* 62, 548–557. <https://doi.org/10.1016/j.jnucene.2013.05.027>.
- D.A.G. Bruggeman, Berechnung verschiedener physikalischer Konstanten von heterogenen Substanzen. I. Dielektrizitätskonstanten und Leitfähigkeiten der Mischkörper aus isotropen Substanzen, *Ann. Phys.* 416 (1935) 636–664. <https://doi.org/10.1002/andp.19354160705>.
- Burke, T., Betzler, B.R., Lee, J.C., Martin, W.R., Pavlou, A., Li, W., Li, Y., 2012. A constrained sampling methodology for TRISO micro spheres with continuous distributions of diameters. *Trans. Am. Nucl. Soc.* 107, 516.
- Chiew, Y.C., Glandt, E.D., 1983. The effect of structure on the conductivity of a dispersion. *J. Colloid Interface Sci.* 94, 90–104. [https://doi.org/10.1016/0021-9797\(83\)90238-2](https://doi.org/10.1016/0021-9797(83)90238-2).
- Demkowicz, P.A., Liu, B., Hunn, J.D., 2019. Coated particle fuel: historical perspectives and current progress. *J. Nucl. Mater.* 515, 434–450. <https://doi.org/10.1016/j.jnucmat.2018.09.044>.
- Fang, M., Di Fulvio, A., 2023. Feasibility of neutron coincidence counting for spent TRISO fuel. *Ann. Nucl. Energy* 193, 110062. <https://doi.org/10.1016/j.jnucene.2023.110062>.
- Folsom, C., Xing, C., Jensen, C., Ban, H., Marshall, D.W., 2015. Experimental measurement and numerical modeling of the effective thermal conductivity of TRISO fuel compacts. *J. Nucl. Mater.* 458, 198–205. <https://doi.org/10.1016/j.jnucmat.2014.12.042>.
- K. Fukuda, K. Hayashi, K. Shiba, Fuel behavior and fission product release under HTGR accident conditions, in: 1990: pp. 197–204.
- Gong, J., Yuan, R., Song, X., Wang, Y., Liu, B., Liu, M., 2023. Numerical analysis of effective thermal conductivity of FCM with multilayer TRISO particle. *Nucl. Mater. Energy* 36, 101501. <https://doi.org/10.1016/j.nme.2023.101501>.
- Haynes, T.A., Battistini, A., Leide, A.J., Liu, D., Jones, L., Shepherd, D., Wenman, M.R., 2023. Peridynamic modelling of cracking in TRISO particles for high temperature reactors. *J. Nucl. Mater.* 576, 154283 <https://doi.org/10.1016/j.jnucmat.2023.154283>.
- Hernandez, R., Folsom, C.P., Woolstenhulme, N.E., Jensen, C.B., Bess, J.D., Gorton, J.P., Brown, N.R., 2020. Review of pool boiling critical heat flux (CHF) and heater rod design for CHF experiments in TREAT. *Prog. Nucl. Energy* 123, 103303. <https://doi.org/10.1016/j.pnucene.2020.103303>.
- IAEA, 1997. Fuel Performance and Fission Product Behaviour in Gas-Cooled Reactors. International Atomic Energy Agency.
- Ji, W., Liang, C., Pusateri, E.N., 2014. Analytical Dancoff factor evaluations for reactor designs loaded with TRISO particle fuel. *Ann. Nucl. Energy* 63, 665–673. <https://doi.org/10.1016/j.jnucene.2013.09.025>.
- Lee, Y., Cho, N.Z., 2014. Three-dimensional single-channel thermal analysis of fully ceramic microencapsulated fuel via two-temperature homogenized model. *Ann. Nucl. Energy* 71, 254–271. <https://doi.org/10.1016/j.jnucene.2014.03.039>.
- Lee, Y., Cho, N.Z., 2015. Steady- and transient-state analyses of fully ceramic microencapsulated fuel loaded reactor core via two-temperature homogenized thermal-conductivity model. *Ann. Nucl. Energy* 76, 283–296. <https://doi.org/10.1016/j.jnucene.2014.09.027>.
- Lee, Y., Cho, B., Cho, N.Z., 2016. Steady- and transient-state analyses of fully ceramic microencapsulated fuel with randomly dispersed tristructural isotropic particles via two-temperature homogenized model—I: theory and method. *Nucl. Eng. Technol.* 48, 650–659. <https://doi.org/10.1016/j.net.2016.02.007>.
- Li, J., She, D., Shi, L., 2021. A comparison study on mechanical models for TRISO fuel particle in HTGR. *Ann. Nucl. Energy* 161, 108484. <https://doi.org/10.1016/j.jnucene.2021.108484>.
- Liu, M., Lee, Y., Rao, D.V., 2018. Development of effective thermal conductivity model for particle-type nuclear fuels randomly distributed in a matrix. *J. Nucl. Mater.* 508, 168–180. <https://doi.org/10.1016/j.jnucmat.2018.05.044>.
- Liu, M., Thurgood, J., Lee, Y., Rao, D.V., 2019. Development of a two-regime heat conduction model for TRISO-based nuclear fuels. *J. Nucl. Mater.* 519, 255–264. <https://doi.org/10.1016/j.jnucmat.2019.04.004>.
- Marsaglia, G., Bray, T.A., 1964. A convenient method for generating normal variables. *SIAM Rev.* 6, 260–264.
- Maxwell, J.C., 1873. *A treatise on electricity and magnetism*. Clarendon Press.
- Petti, D.A., Buongiorno, J., Maki, J.T., Hobbins, R.R., Miller, G.K., 2003. Key differences in the fabrication, irradiation and high temperature accident testing of US and German TRISO-coated particle fuel, and their implications on fuel performance. *Nucl. Eng. Des.* 222, 281–297. [https://doi.org/10.1016/S0029-5493\(03\)00033-5](https://doi.org/10.1016/S0029-5493(03)00033-5).
- Pietrak, K., Wiśniewski, T.S., 2015. A review of models for effective thermal conductivity of composite materials. *J. Power Technol.* 95, 14–24.
- J.J. Powers, W.J. Lee, F. Venneri, L.L. Snead, C.K. Jo, D.H. Hwang, J.H. Chun, Y.M. Kim, K.A. Terrani, Fully Ceramic Microencapsulated (FCM) Replacement Fuel for LWRs, 2013. <https://doi.org/10.2172/1087039>.
- Powers, J.J., Wirth, B.D., 2010. A review of TRISO fuel performance models. *J. Nucl. Mater.* 405, 74–82. <https://doi.org/10.1016/j.jnucmat.2010.07.030>.
- Terrani, K.A., Snead, L.L., Gehin, J.C., 2012. Microencapsulated fuel technology for commercial light water and advanced reactor application. *J. Nucl. Mater.* 427, 209–224. <https://doi.org/10.1016/j.jnucmat.2012.05.021>.
- Umeda, M., Sugiyama, T., Nagase, F., Fuketa, T., Ueta, S., Sawa, K., 2010. Behavior of coated fuel particle of high-temperature gas-cooled reactor under reactivity-initiated accident conditions. *J. Nucl. Sci. Technol.* 47, 991–997. <https://doi.org/10.3327/jnst.47.991>.
- Wang, M., Bu, S., Zhou, B., Li, Z., Chen, D., 2023a. Multi-scale heat conduction models with improved equivalent thermal conductivity of TRISO fuel particles for FCM fuel. *Nucl. Eng. Technol.* 55, 1140–1151. <https://doi.org/10.1016/j.net.2022.12.001>.
- Wang, M., Zhou, B., Bu, S., Li, Z., Chen, D., Ma, Z., Zhang, L., 2023b. A multi-annulus heat conduction model for predicting the peak temperature of nuclear fuels with randomly dispersed TRISO particles. *Prog. Nucl. Energy* 158, 104602. <https://doi.org/10.1016/j.pnucene.2023.104602>.
- Woolstenhulme, N., Fleming, A., Holschuh, T., Jensen, C., Kamerman, D., Wachs, D., 2020. Core-to-specimen energy coupling results of the first modern fueled experiments in TREAT. *Ann. Nucl. Energy* 140, 107117. <https://doi.org/10.1016/j.jnucene.2019.107117>.
- Zhang, C., Liu, J., Li, X., Wei, C., Zheng, C., Liao, H., Li, C., Li, Y., Wu, Y., Su, G.H., 2023. Multi-objective optimization design of TRISO-based fully ceramic microencapsulated fuel. *J. Nucl. Mater.* 585, 154650 <https://doi.org/10.1016/j.jnucmat.2023.154650>.